PERGAMON Computers and Mathematics with Applications 40 (2000) 345–357

An International Journal
computers & mathematics
with applications

www.elsevier.nl/locate/camwa

Multi-Nephron and Multi-Vasa Recta Models of the Inner Medullary Renal Concentrating Mechanism

I. H. MOON AND R. P. TEWARSON
Institute of Mathematical Modeling
Department of Applied Mathematics and Statistics
State University of New York
Stony Brook, NY 11794-3600, U.S.A.

(Received December 1998; accepted January 1999)

Abstract—Three multi-nephron vasa recta models of the renal concentrating mechanism are presented. These models are physiologically more realistic than our shunt vasa recta models. It is also shown that by considering the effects of fractional transmural fluxes between tubes and role of the interstitium in the permeability values, these models lead to significant improvements in collecting duct urea and salt concentration ratios.

Keywords—Numerical solutions, Renal concentrating mechanism, Multi-nephron and multi-vasa recta models.

1. INTRODUCTION

Conceptual insight into renal function has been significantly increased by mathematical models of the kidney. Edwards and Pallone [1] have given an excellent justification for the development of mathematical models, "Because experimental approaches to the renal medulla are technically limited, mathematical simulations are required to obtain insight into equations that cannot otherwise be readily addressed." In the rat, each kidney contains 30,000 to 35,000 nephrons and an average of six nephrons drain into a cortical collecting duct. Approximately, 20 papillary ducts in rat empty into the pelvis [2]. The loops (descending Henle's loops DHL, and ascending Henle's loops AHL, vasa recta (descending vasa recta DVR, ascending vasa recta AVR) turn around at different depths in the inner medulla. This is modeled by incorporating shunts between the descending and ascending tubes (e.g., see our seven tube model [3]). The development of progressively realistic models also requires that shunts in the Henle's loops and vasa recta be replaced by multi-nephron and multi-vasa recta models. The number of Henle's loops, collecting duct (CD) and vasa recta (VR) are assumed to decrease exponentially in the inner medulla [4]. It has been pointed out that the distribution of various nephron lengths plays an important role in concentrating abilities [5–7]. Since multi-nephron central core models [8–10] generally led to better

0898-1221/00/$ - see front matter Typeset by AMS-TEX
PII: S0898-1221(00)00165-6

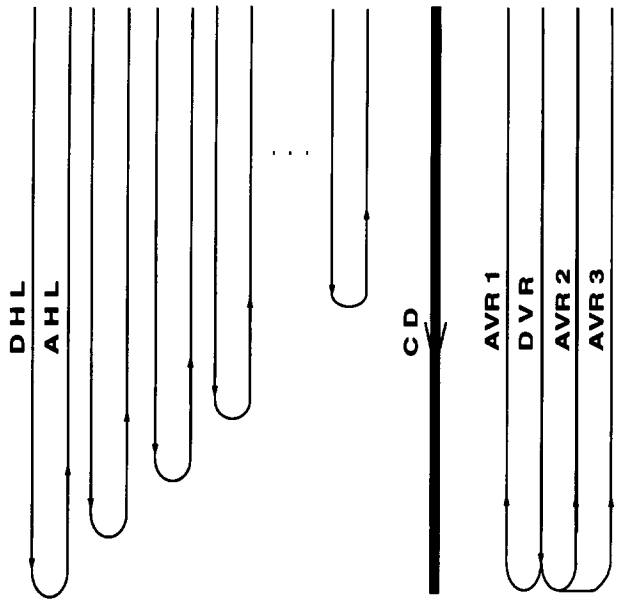

Figure 1. Multi-DHL-AHL, collecting duct, and shunt vasa recta model (MN1).

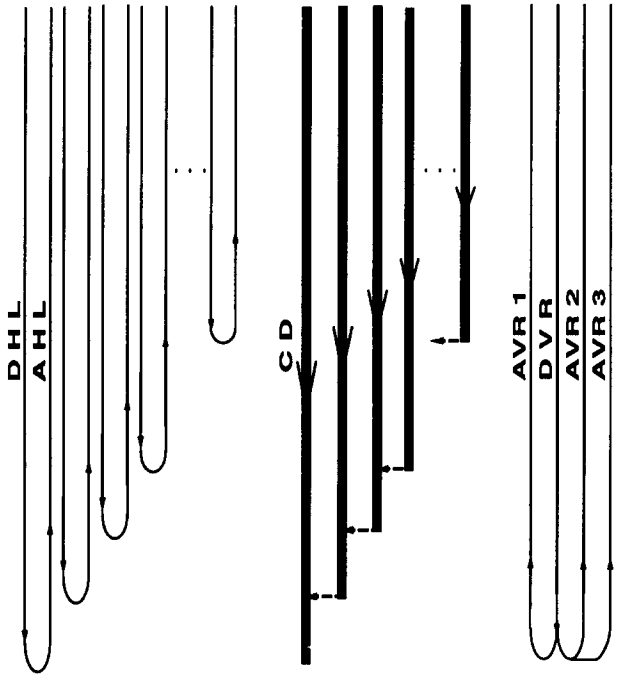

Figure 2. Multi-DHL-AHL-CD and shunt vasa recta model (MN2).

concentrations profiles than central core shunt models, we used model $M1$ (see [3, Figure 3]) as a basic shunt model to develop multi-nephron and multi-vasa recta models. In this paper, we describe three models: MN1 (see Figure 1), MN2 (see Figure 2), and MN3 (see Figure 3).

2. MULTI-DHL-AHL, COLLECTING DUCT, AND SHUNT VASA RECTA MODEL (MN1)

This model, MN1, consists of nl, DHLs, (and AHLs) of different lengths, one CD, one DVR and *three* AVRs. Each DHL turns at a different level and has a weight factor λ_i which reflects the actual number of DHL turning at that level. In DHL, AHL, CD, and VR, the transport of

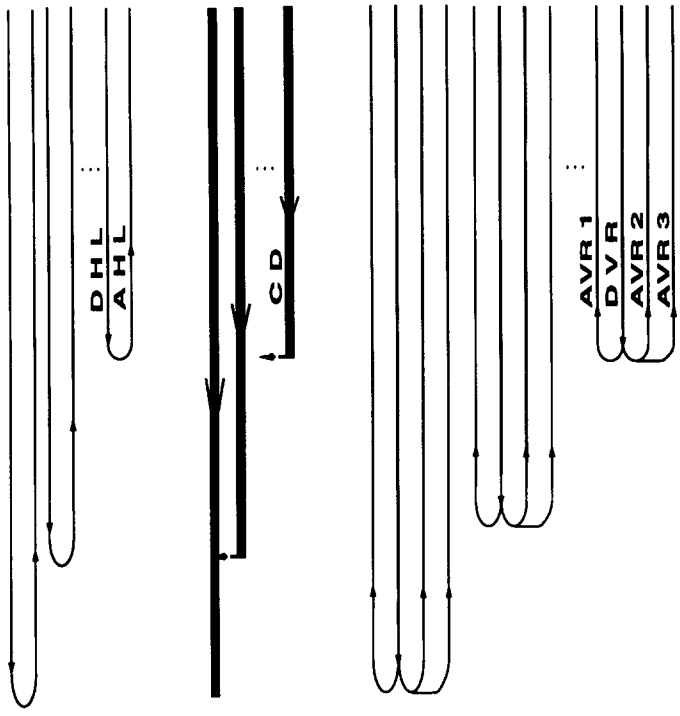

Figure 3. Multi-DHL-AHL-CD and shunt vasa recta model (MN3).

salt, urea, and water are described by the following differential equations.

DHL AND AHL EQUATIONS.

$$\frac{dF_{iv}^{\mathrm{da}}}{dx} + \lambda_i \, J_{iv}^{\mathrm{da}}(x) = 0, \qquad i = 1, 2, \ldots, \mathrm{nl}, \tag{1}$$

$$\frac{d\left(F_{iv}^{\mathrm{da}} C_{ik}^{\mathrm{da}}\right)}{dx} + \lambda_i \, J_{ik}^{\mathrm{da}}(x) = 0, \qquad i = 1, 2, \ldots, \mathrm{nl}; \quad k = s, u. \tag{2}$$

CD EQUATIONS.

$$\frac{dF_{1v}^{\mathrm{cd}}}{dx} + \mathrm{ncd}(x) J_{1v}^{\mathrm{cd}}(x) = 0, \tag{3}$$

$$\frac{d\left(F_{1v}^{\mathrm{cd}} C_{1k}^{\mathrm{cd}}\right)}{dx} + \mathrm{ncd}(x) J_{1k}^{\mathrm{cd}}(x) = 0, \qquad k = s, u. \tag{4}$$

DVR EQUATIONS.

$$\frac{dF_{1v}^{\mathrm{dv}}}{dx} + \mathrm{nvr}(x) J_{1v}^{\mathrm{dv}}(x) = 0, \tag{5}$$

$$\frac{d\left(F_{1v}^{\mathrm{dv}} C_{1k}^{\mathrm{dv}}\right)}{dx} + \mathrm{nvr}(x) J_{1k}^{\mathrm{dv}}(x) = 0, \qquad k = s, u. \tag{6}$$

AVR EQUATIONS.

$$\frac{dF_{1v}^{\mathrm{av}}}{dx} + J_{1v}^{\mathrm{av}}(x) = 0, \qquad \mathrm{av} = 1, 2, 3, \tag{7}$$

$$\frac{d\left(F_{1v}^{\mathrm{av}} C_{1k}^{\mathrm{av}}\right)}{dx} + J_{1k}^{\mathrm{av}}(x) = 0, \qquad \mathrm{av} = 1, 2, 3, \quad k = s, u. \tag{8}$$

The transmural fluxes are given by

$$J_{iv}^{l}(x) = h_{iv}^{l}(x) \sum_{k} RT \left[C_{ik}^{\mathrm{av}}(x) - C_{ik}^{l}(x)\right] \sigma_{lk}(x), \qquad k = s, u, \quad (9)$$

$$J_{ik}^{l}(x) = J_{iv}^{l}(x) \left[1 - \sigma_{lk}(x)\right] \frac{C_{ik}^{l}(x) + C_{ik}^{\mathrm{av}}(x)}{2} + h_{ik}^{l}(x) \left[C_{ik}^{l}(x) - C_{ik}^{\mathrm{av}}(x)\right], \qquad k = s, u, \quad (10)$$

where σ_{lk} is the Staverman reflection coefficient of the wall of the l^{th} type of tubule, av = ascending vasa recta, l = descending/ascending Henle's limbs (da), collecting duct (cd) and descending vasa recta (dv), for the k^{th} solute, h_{ik}^{l} is its passive permeability for the i^{th} tube and l^{th} type of tubule and the k^{th} solute, h_{iv}^{l} is its hydraulic permeability coefficient, R is the gas constant, and T is the absolute temperature.

In addition, *global mass conservation* (GMC) requires that both the sum of the volume fluxes and the sum of the solute fluxes at each level remain constant, viz.,

$$\sum_{\mathrm{av}=1}^{3} J_{1v}^{\mathrm{av}}(x) + \mathrm{nvr}(x) J_{1v}^{\mathrm{dv}}(x) + \sum_{i=1}^{\mathrm{nl}} \lambda_i J_{iv}^{\mathrm{da}}(x) + \mathrm{ncd}(x) J_{1v}^{\mathrm{cd}}(x) = 0, \quad (11)$$

$$\sum_{\mathrm{av}=1}^{3} J_{1k}^{\mathrm{av}}(x) + \mathrm{nvr}(x) J_{1k}^{\mathrm{dv}}(x) + \sum_{i=1}^{\mathrm{nl}} \lambda_i J_{ik}^{\mathrm{da}}(x) + \mathrm{ncd}(x) J_{1k}^{\mathrm{cd}}(x) = 0, \qquad k = s, u. \quad (12)$$

Let x be the normalized depth in the inner medulla (IM), with $x = 0$ at the top of IM and $x = 1$ at the papillary tip of IM. We want to approximate the continuous distribution of the loops with a model of finite nl types of loops classified according to their turning points. Each DHL makes a hairpin turn at $la(i) = (\mathrm{nl} + 1 - i) \times \mathrm{chops} + 1$ for the i^{th} loop to become AHL. If we set $h = 1/n$, $n = la(1) - 1$, $x_j = (j-1) \times h$ where $j = 1, 2, \ldots, n+1$, then all points are $0 = x_1 < x_2 < \cdots < x_n < x_{n+1} = 1$, with the i^{th} type of loop turning at $x_{la(i)}$. To determine the weight factor λ_i for the i^{th} type of loop, we have

$$\lambda_1 = \mathrm{nl}p(\mathrm{nl}), \quad (13)$$

$$\lambda_2 = \mathrm{nl}p(\mathrm{nl} - 1) - \mathrm{nl}p(\mathrm{nl}), \quad (14)$$

$$\lambda_3 = \mathrm{nl}p(\mathrm{nl} - 2) - \mathrm{nl}p(\mathrm{nl} - 1), \quad (15)$$

$$\vdots$$

$$\lambda_{\mathrm{nl}-1} = \mathrm{nl}p(2) - \mathrm{nl}p(3), \quad (16)$$

$$\lambda_{\mathrm{nl}} = \mathrm{nl}p(1) - \mathrm{nl}p(2), \quad (17)$$

where nl denotes total number of loops and $\mathrm{nl}p(i) = 2.0 \times e^{-12.13 \times 0.4 \times h \times (i-1)}$, $i = 1, \ldots, \mathrm{nl}$, [4].

As shown in [11], integrating (1)–(8) and using the boundary conditions, we get a system of nonlinear algebraic equations, which can be written as

$$f(y, z) = 0, \quad (18)$$

$$g(y, z) = 0, \quad (19)$$

where $y = (C_{ikj}^{l}), k = s, u$, $i = 1, \ldots, \mathrm{nl}$, for l = DHL and AHL, $i = 1$ for l = CD; for l = DHL, $j = 2, \ldots, la(i)$, and for l = AHL, $j = la(i) - 1, \ldots, 1$; $z = (F_{1vj}^{\mathrm{dv}}, C_{1kj}^{\mathrm{dv,av}})$, $k = s, u$; for av $= 1, 2, 3$, $j = 1, \ldots, la(1) - 1$, and for dv, $j = 2, \ldots, la(1)$. Therefore, in equations (18) and (19), for this model, $f, y \in R^{[2 \times \mathrm{nl} \times (\mathrm{nl}+2) \times \mathrm{chops}]}$ and $g, z \in R^{[9 \times \mathrm{nl} \times \mathrm{chops}]}$. The basic equations and variables are the ones associated with DVR, AVR1, AVR2, and AVR3. As shown in [11,12], the nonbasic variables y are expressed as functions of the basic variables z by solving the nonbasic equations $f(y(z), z) = 0$ for $y(z)$. This leads to an efficient algorithm for the basic equations $g(y(z), z) = 0$ for z.

3. MULTI-DHL-AHL-CD AND SHUNT VASA RECTA MODEL (MN2)

This model, MN2, consists of nl DHLs (and AHLs) of different lengths, nc CDs of different lengths, one DVR and *three* AVRs. Each DHL of this model has same structure as MN1. Each CD has a weight factor η_i. In this model, equations (3), (4), (11), and (12) are changed as follows.

CD EQUATIONS.

$$\frac{dF_{iv}^{\mathrm{cd}}}{dx} + \eta_i J_{iv}^{\mathrm{cd}}(x) = 0, \qquad i = 1, 2, \ldots, \mathrm{nc}, \tag{20}$$

$$\frac{d(F_{iv}^{\mathrm{cd}} C_{i,k}^{\mathrm{cd}})}{dx} + \eta_i J_{ik}^{\mathrm{cd}}(x) = 0, \qquad i = 1, 2, \ldots, \mathrm{nc}, \quad k = s, u. \tag{21}$$

GMC EQUATIONS.

$$\sum_{\mathrm{av}=1}^{3} J_{1v}^{\mathrm{av}}(x) + \mathrm{nvr}(x) J_{1v}^{\mathrm{dv}}(x) + \sum_{i=1}^{\mathrm{nl}} \lambda_i J_{iv}^{\mathrm{da}}(x) + \sum_{i=1}^{\mathrm{nc}} \eta_i J_{iv}^{\mathrm{cd}}(x) = 0, \tag{22}$$

$$\sum_{\mathrm{av}=1}^{3} J_{1k}^{\mathrm{av}}(x) + \mathrm{nvr}(x) J_{1k}^{\mathrm{dv}}(x) + \sum_{i=1}^{\mathrm{nl}} \lambda_i J_{ik}^{\mathrm{da}}(x) + \sum_{i=1}^{\mathrm{nc}} \eta_i J_{ik}^{\mathrm{cd}}(x) = 0, \qquad k = s, u. \tag{23}$$

Each CD is of length $la(i) = (\mathrm{nc} + 1 - i) \times \mathrm{chops} + 1$. To determine the weight factor η_i for the i^{th} type of CD, we have

$$\eta_1 = \mathrm{ncd}(\mathrm{nc}), \tag{24}$$

$$\eta_2 = \mathrm{ncd}(\mathrm{nc} - 1) - \mathrm{ncd}(\mathrm{nc}), \tag{25}$$

$$\eta_3 = \mathrm{ncd}(\mathrm{nc} - 2) - \mathrm{ncd}(\mathrm{nc} - 1), \tag{26}$$

$$\vdots$$

$$\eta_{\mathrm{nc}-1} = \mathrm{ncd}(2) - \mathrm{ncd}(3), \tag{27}$$

$$\eta_{\mathrm{nc}} = \mathrm{ncd}(1) - \mathrm{ncd}(2), \tag{28}$$

where nc denotes total number of CDs and $\mathrm{ncd}(i) = 1.0 \times e^{-8.66 \times 0.4 \times h \times (i-1)}$, $i = 1, \ldots, \mathrm{nc}$, [4].

For this model, we let $y = (C_{ikj}^{l})$, $k = s, u$, $i = 1, \ldots, \mathrm{nl}$, for l = DHL, AHL, and CD; for l=DHL and CD, $j = 2, \ldots, la(i)$, and for l = AHL, $j = la(i) - 1, \ldots, 1$; $z = (F_{1vj}^{\mathrm{dv}}, C_{1kj}^{\mathrm{dv,av}})$, $k = s, u$; for av $= 1, 2, 3$, $j = 1, \ldots, la(1) - 1$, and for dv, $j = 2, \ldots, la(1)$. Therefore, in equations (18) and (19), $f, y \in R^{[3 \times \mathrm{nl} \times (\mathrm{nl}+1) \times \mathrm{chops}]}$ and $g, z \in R^{[9 \times \mathrm{nl} \times \mathrm{chops}]}$.

4. MULTI-DHL-AHL-CD-VASA RECTA MODEL (MN3)

This model, MN3, consists of nl DHLs (and AHLs) of different lengths, nc CDs of different lengths, nd DVRs and na *three* AVRs of different lengths. Each DHL and CD of this model has same structure as MN2. Each DVR turns at a different level into *three* AVRs and has a weight factor ω_i which reflects the actual number of DVRs turning at that level. In this model, equations (3)–(8), (11), and (12) are changed as follows.

CD EQUATIONS.

$$\frac{dF_{iv}^{\mathrm{cd}}}{dx} + \eta_i J_{iv}^{\mathrm{cd}}(x) = 0, \qquad i = 1, 2, \ldots, \mathrm{nc}, \tag{29}$$

$$\frac{d\left(F_{iv}^{\mathrm{cd}} C_{i,k}^{\mathrm{cd}}\right)}{dx} + \eta_i J_{ik}^{\mathrm{cd}}(x) = 0, \qquad i = 1, 2, \ldots, \mathrm{nc}, \quad k = s, u, \tag{30}$$

DVR EQUATIONS.

$$\frac{dF_{iv}^{\mathrm{dv}}}{dx} + \omega_i J_{iv}^{\mathrm{dv}}(x) = 0, \qquad i = 1, 2, \ldots, \mathrm{nd}, \tag{31}$$

$$\frac{d\left(F_{iv}^{\mathrm{dv}} C_{ik}^{\mathrm{dv}}\right)}{dx} + \omega_i J_{ik}^{\mathrm{dv}}(x) = 0, \qquad i = 1, 2, \ldots, \mathrm{nd}, \tag{32}$$

AVR EQUATIONS.

$$\frac{dF_{iv}^{\mathrm{av}}}{dx} + J_{iv}^{\mathrm{av}}(x) = 0, \qquad i = 1, 2, \ldots, \mathrm{na}, \tag{33}$$

$$\frac{d(F_{iv}^{\mathrm{av}} C_{ik}^{\mathrm{av}})}{dx} + J_{ik}^{\mathrm{av}}(x) = 0, \qquad i = 1, 2, \ldots, \mathrm{na}, \quad k = s, u, \tag{34}$$

GMC EQUATIONS.

$$\sum_{i=1}^{\mathrm{na}} J_{iv}^{\mathrm{av}}(x) + \sum_{i=1}^{\mathrm{nd}} \omega_i J_{iv}^{\mathrm{dv}}(x) \sum_{i=1}^{\mathrm{nc}} \eta_i J_{iv}^{\mathrm{cd}}(x) = 0, \tag{35}$$

$$\sum_{i=1}^{\mathrm{na}} J_{ik}^{\mathrm{av}}(x) + \sum_{i=1}^{\mathrm{nd}} \omega_i J_{ik}^{\mathrm{dv}}(x) \sum_{i=1}^{\mathrm{nc}} \eta_i J_{ik}^{\mathrm{cd}}(x) = 0, \qquad k = s, u. \tag{36}$$

Each DVR makes a hairpin turn at $la(i) = (\mathrm{nd} + 1 - i) \times \mathrm{chops} + 1$, for the i^{th} loop to become *three* AVRs. Each CD and DHL lengths are the same as in MN2. To determine the weight factor ω_i for the i^{th} type of VR, we have

$$\omega_1 = \mathrm{nvr}(\mathrm{nd}), \tag{37}$$

$$\omega_2 = \mathrm{nvr}(\mathrm{nd} - 1) - \mathrm{nvr}(\mathrm{nd}), \tag{38}$$

$$\omega_3 = \mathrm{nvr}(\mathrm{nd} - 2) - \mathrm{nvr}(\mathrm{nd} - 1), \tag{39}$$

$$\vdots$$

$$\omega_{\mathrm{nd}-1} = \mathrm{nvr}(2) - \mathrm{nvr}(3), \tag{40}$$

$$\omega_{\mathrm{nd}} = \mathrm{nvr}(1) - \mathrm{nvr}(2), \tag{41}$$

where nd denotes total number of VRs and $\mathrm{nvr}(i) = 4.0 \times e^{-12.13 \times 0.4 \times h \times (i-1)}$, where $i = 1, \ldots, \mathrm{nd}$, [4].

For this model, we let $y = (C_{ikj}^{l})$, $k = s, u$, $i = 1, \ldots, \mathrm{nl}$, for $l = \mathrm{DHL}$, AHL, and CD; for $l = \mathrm{DHL}$ and CD, $j = 2, \ldots, la(i)$ and for $l = \mathrm{AHL}$, $j = la(i) - 1, \ldots, 1$; $z = (F_{ivj}^{\mathrm{dv}}, C_{ikj}^{\mathrm{dv,av}})$, $k = s, u$, $i = 1, \ldots, \mathrm{na}$. Therefore, in equations (18) and (19), $g, z \in R^{[9 \times ((\mathrm{nl}-1) \times \mathrm{nl} - (\mathrm{nl} \times \mathrm{nl} - 3 \times \mathrm{nl})/2) \times \mathrm{chops}]}$ and $f, y \in R^{[3 \times \mathrm{nl} \times (\mathrm{nl}+1) \times \mathrm{chops}]}$.

5. MODEL ANALYSIS

In Table 1, we have shown the permeabilities and reflection coefficients.

Let Υ_{il} represent the fractions for transmural fluxes between i and l tubes. The sum of Υ_{il}, $i = \mathrm{DHL}$, AHL, CD, and DVR has to be equal to 1.0.

$$\Upsilon_{\mathrm{DHL,AVR1}} + \Upsilon_{\mathrm{DHL,AVR2}} + \Upsilon_{\mathrm{DHL,AVR3}} = 1.0, \tag{42}$$

$$\Upsilon_{\mathrm{AHL,AVR1}} + \Upsilon_{\mathrm{AHL,AVR2}} = 1.0, \tag{43}$$

$$\Upsilon_{\mathrm{CD,AVR2}} + \Upsilon_{\mathrm{CD,AVR3}} = 1.0, \tag{44}$$

$$\Upsilon_{\mathrm{DVR,AVR1}} + \Upsilon_{\mathrm{DVR,AVR2}} + \Upsilon_{\mathrm{DVR,AVR3}} = 1.0. \tag{45}$$

Table 1. Parameter values with standard deviations.

Unnormalized Values

	$h_w \times 10^{-5}$ cm × atm^{-1} × s^{-1}	$h_s \times 10^{-5}$ cm × s^{-1}	$h_u \times 10^{-5}$ cm × s^{-1}	σ_s	σ_u	References
DHL-Upper	25.08 ± 6.47	3.50 ± 1.2	13.50 ± 6.5	0.99 ± 0.04	0.97 ± 0.04	[13]
-Lower	25.08 ± 6.47	3.50 ± 1.2	13.50 ± 6.5	0.99 ± 0.04	0.97 ± 0.04	[13]
AHL-Upper	0.18 ± 0.144	79.60 ± 3.6	22.80 ± 4.5	1	1	[14]
-Lower	0.18 ± 0.144	79.60 ± 3.6	22.80 ± 4.5	1	1	[14]
CD-Upper	1.095 ± 0.37	0.00	4.10 ± 0.7	1.00 ± 0.05	1	[15]
-Lower	1.535 ± 0.24	1.18 ± 0.24	69.20 ± 15.2	1.00 ± 0.05	1	[15,16]
DVR-Upper	266.00	75.00± 10.00	76.00 ±11.00	0.017	0.07	[17–19]
-Lower	266.00	75.00± 10.00	76.00 ±11.00	0.017	0.07	[17–19]

Table 2. The fractions for transmural fluxes between i and l tubes.

$\Upsilon_{\mathrm{DHL,AVR1}}$	$\Upsilon_{\mathrm{DHL,AVR2}}$	$\Upsilon_{\mathrm{AHL,AVR1}}$	$\Upsilon_{\mathrm{CD,AVR2}}$	$\Upsilon_{\mathrm{DVR,AVR1}}$	$\Upsilon_{\mathrm{DVR,AVR2}}$
0.33	0.33	0.5	0.5	0.33	0.33

The values for the fractions for transmural fluxes between tubes are shown in Table 2.

In view of [13, Figure 1d, p. 540], it seems reasonable to assume that DVR is closer to DHL and CD than other tubes. Let $\Upsilon_{i,\mathrm{DVR}}$, i = DHL, and CD, represent the fractions of total transmural fluxes between DHL and DVR; CD and DVR, then (42), (43), and (45) are changed,

$$\Upsilon_{\mathrm{DHL,AVR1}} + \Upsilon_{\mathrm{DHL,AVR2}} + \Upsilon_{\mathrm{DHL,AVR3}} + \Upsilon_{\mathrm{DHL,DVR}} = 1.0, \tag{46}$$

$$\Upsilon_{\mathrm{AHL,AVR1}} + \Upsilon_{\mathrm{AHL,AVR2}} + \Upsilon_{\mathrm{AHL,DVR}} = 1.0, \tag{47}$$

$$\Upsilon_{\mathrm{DVR,AVR1}} + \Upsilon_{\mathrm{DVR,AVR2}} + \Upsilon_{\mathrm{DVR,AVR3}} + \Upsilon_{\mathrm{DHL,DVR}} + \Upsilon_{\mathrm{AHL,DVR}} = 1.0. \tag{48}$$

We derived entering volume flows for each DHL, CD, and DVR as follows.

DHL:

$$\theta_i = \frac{\lambda_i}{\sum_{i=1}^{\mathrm{nl}} \lambda_i}, \qquad i = 1, 2, \ldots, \mathrm{nl}, \tag{49}$$

$$F_{iv}^{\mathrm{DHL}}(0) = \theta_i \times 1.0 \times 10^{-7}\mathrm{ml/sec}, \qquad i = 1, 2, \ldots, \mathrm{nl}, \tag{50}$$

CD:

$$\phi_i = \frac{\eta_i}{\sum_{i=1}^{\mathrm{nc}} \eta_i}, \qquad i = 1, 2, \ldots, \mathrm{nc}, \tag{51}$$

$$F_{iv}^{\mathrm{cd}}(0) = \phi_i \times 0.1 \times 10^{-7}\mathrm{ml/sec}, \qquad i = 1, 2, \ldots, \mathrm{nc}, \tag{52}$$

DVR:

$$\psi_i = \frac{\omega_i}{\sum_{i=1}^{\mathrm{nd}} \omega_i}, \qquad i = 1, 2, \ldots, \mathrm{nd}, \tag{53}$$

$$F_{iv}^{\mathrm{DVR}}(0) = \psi_i \times 2.0 \times 10^{-7}\mathrm{ml/sec}, \qquad i = 1, 2, \ldots, \mathrm{nd}, \tag{54}$$

and variations in permeabilities for every tube in DHL, AHL, CD, and DVR are

$$\widehat{h(i)}_{\xi}^{\varepsilon} = h_{\xi}^{\varepsilon}(\min) + \Lambda_i \times 2.0 \times \Delta h_{\xi}^{\varepsilon}, \qquad i = 1, 2, \ldots, \mathrm{nl}, (\text{or nc}, \text{or nd}), \tag{55}$$

Table 3. Estimated Boundary Values from [2,14].

	DHL	CD	DVR
Volume Flow, 10^{-7} ml/sec	1.000	0.100	2.000
Salt Concentration, mmol/ml	0.237	0.100	0.203
Urea Concentration, mmol/ml	0.045	0.295	0.774

Table 4. Osmolality and concentration ratios between values at $x = 1$ and $x = 0$ with parameters, transmural flux fractions, and boundary values from Tables 1–3.

		MN1											
		DHL			cd			DHL			cd		
nl	chops	Osm.	Salt	Urea	Osm.	Salt	Urea	Osm.	Salt	Urea	Osm.	Salt	Urea
60	1	1.748	1.693	2.283	1.807	1.823	1.797						
80	1	1.745	1.688	2.286	1.804	1.765	1.828						
40	2							1.801	1.744	2.346	1.855	1.979	1.778
100	1	1.757	1.699	2.308	1.816	1.744	1.860						
120	1	1.773	1.714	2.335	1.831	1.738	1.889						
60	2							1.751	1.695	2.288	1.809	1.823	1.801
40	3							1.801	1.744	2.346	1.855	1.976	1.780
140	1	1.791	1.731	2.363	1.848	1.739	1.915						
160	1	1.808	1.747	2.390	1.865	1.744	1.939						
80	2							1.748	1.692	2.291	1.807	1.766	1.833
40	4							1.801	1.744	2.346	1.855	1.975	1.781
80	1	1.824	1.763	2.416	1.880	1.750	1.960						
60	3							1.752	1.696	2.290	1.810	1.822	1.803
200	1	1.840	1.777	2.440	1.895	1.758	1.979						
100	2							1.760	1.702	2.313	1.819	1.746	1.864
40	5							1.801	1.744	2.346	1.855	1.973	1.781
220	1	1.854	1.791	2.463	1.908	1.765	1.997						
240	1	1.868	1.804	2.483	1.921	1.773	2.013						
120	2							1.776	1.717	2.340	1.834	1.740	1.893
80	3							1.749	1.693	2.293	1.808	1.767	1.834
60	4							1.753	1.696	2.290	1.811	1.822	1.804
40	6							1.801	1.744	2.347	1.855	1.972	1.782

where $\xi = w, s, u$, $\Lambda_i = \theta_i$ for $\varepsilon =$ DHL, AHL; $\Lambda_i = \phi_i$ for $\varepsilon =$ CD; $\Lambda_i = \psi_i$ for $\varepsilon =$ DVR, and Δh_ξ^ε denote the standard deviations. However, permeabilities from top to bottom are the same in each tube.

The interstitium is a gelatinous material which is rich in glycosaminoglycans, which present considerable resistance to bulk flow of water and diffusion of small solutes [13]. Also, the edges of the interstitial cells block portions of the tubule wall [13]. It may be assumed that under different functional conditions (e.g., changes in tubular and vascular volume), the shape of the processes, and thus, the extent of covering, varies. If the resistances in the interstitium to the molecules is proportional to their molecular weights, water (w) ≈ 18, salt (s) ≈ 58, urea (u) ≈ 60, and furthermore, the interstitium increases relatively in size say d_ξ, $\xi = w, s, u$, times, then the ramp functions for the variations in permeabilities from top to bottom in each tube are

$$\overline{h(i)}_{j,\xi}^{\varepsilon} = \widehat{h(i)}_{\xi}^{\varepsilon} \times \left[1.0 - d_\xi \times \frac{j-1}{la(i)-1}\right], \qquad j = 1, 2, \ldots, la(i), \tag{56}$$

where $i = 1, \ldots,$ nl for $\varepsilon =$ DHL, AHL; $i = 1, \ldots,$ nc for $\varepsilon =$ CD; $i = 1, \ldots,$ nd for $\varepsilon =$ DVR; $0.1 \le d_u \le 0.3$, $d_w = d_u \times 18/60$, and $d_s = d_u \times 58/60$.

6. COMPUTATIONAL RESULTS

In Table 4, we have shown the results from MN1 using the permeabilities shown in Table 1. The values for the fractions for transmural fluxes are shown in Table 2, and the boundary values are given in Table 3. When we increased nl (number of DHLs and AHLs), CD urea concentration ratios also increased. However, as we increased the number of chops for the same number of loops, CD urea concentration ratios did not change.

Using various fractions for the transmural fluxes between the tubes from MN1, we get the results shown in Table 5. The first line is the result in Table 4 corresponding to nl = 40 and chops = 2, and d, ah, cd, dv, 1, and 2 denote, respectively, DHL, AHL, CD, DVR, AVR1, and AVR2.

In Table 6, we have shown the results from MN2 using parameters, transmural flux fractions, and boundary values from Tables 1–3. When we increased the number of loops and the number of CDs, CD urea concentration ratios also increased. However, as we increased chops with the same number of loops and number of CDs, CD urea concentration ratios did not change.

Table 5. Osmolality and concentration ratios between values at $x = 1$ and $x = 0$ with parameters and boundary values from Tables 1 and 3.

MN1													
								DHL			CD		
$\alpha_{d,1}$	$\alpha_{d,2}$	$\alpha_{ah,1}$	$\alpha_{cd,2}$	$\alpha_{dv,1}$	$\alpha_{dv,2}$	$\alpha_{d,dv}$	$\alpha_{cd,dv}$	Osm.	Salt	Urea	Osm.	Salt	Urea
0.33	0.33	0.5	0.5	0.33	0.33	0.0	0.0	1.801	1.744	2.346	1.855	1.979	1.778
0.33	0.33	0.5	0.375	0.25	0.25	0.0	0.25	1.823	1.764	2.382	1.877	1.974	1.817
0.25	0.25	0.5	0.5	0.25	0.25	0.25	0.0	1.874	1.801	2.571	1.915	2.023	1.848

Table 6. Osmolality and concentration ratios between values at $x = 1$ and $x = 0$ with parameters, transmural flux fractions, and boundary values from Tables 1–3.

		MN2											
		DHL			cd			DHL			cd		
nl	chops	Osm.	Salt	Urea	Osm.	Salt	Urea	Osm.	Salt	Urea	Osm.	Salt	Urea
40	1	1.751	1.697	2.270	1.781	1.833	1.748						
60	1	1.708	1.655	2.223	1.748	1.718	1.767						
80	1	1.708	1.654	2.230	1.753	1.684	1.796						
40	2							1.748	1.694	2.267	1.777	1.825	1.747
100	1	1.721	1.665	2.253	1.768	1.675	1.826						
120	1	1.737	1.680	2.281	1.786	1.678	1.853						
60	2							1.710	1.656	2.225	1.750	1.718	1.770
40	3							1.748	1.694	2.266	1.777	1.823	1.749
140	1	1.755	1.697	2.309	1.804	1.684	1.878						
160	1	1.771	1.713	2.336	1.821	1.693	1.899						
80	2							1.711	1.656	2.234	1.756	1.685	1.799
40	4							1.747	1.693	2.266	1.777	1.821	1.749
180	1	1.787	1.728	2.361	1.837	1.702	1.920						
60	3							1.710	1.657	2.227	1.750	1.717	1.771
200	1	1.803	1.742	2.384	1.851	1.712	1.937						
100	2							1.723	1.668	2.258	1.771	1.677	1.829
40	5							1.747	1.693	2.266	1.777	1.820	1.750
220	1	1.817	1.755	2.406	1.865	1.721	1.954						

Table 7. Osmolality and concentration ratios between values at $x = 1$ and $x = 0$ with parameters and boundary values from Tables 1 and 3.

MN2													
								DHL			cd		
$\alpha_{d,1}$	$\alpha_{d,2}$	$\alpha_{ah,1}$	$\alpha_{cd,2}$	$\alpha_{dv,1}$	$\alpha_{dv,2}$	$\alpha_{d,dv}$	$\alpha_{cd,dv}$	Osm.	Salt	Urea	Osm.	Salt	Urea
0.33	0.33	0.5	0.5	0.33	0.33	0.0	0.0	1.751	1.697	2.270	1.781	1.833	1.748
0.25	0.25	0.5	0.5	0.25	0.25	0.25	0.0	1.716	1.663	2.218	1.775	1.802	1.759
0.33	0.33	0.5	0.375	0.25	0.25	0.0	0.25	1.791	1.735	2.333	1.826	1.850	1.812

Table 8. Osmolality and concentration ratios between values at $x = 1$ and $x = 0$ with parameters, transmural flux fractions, and boundary values from Tables 1–3.

		MN3											
		DHL			cd			DHL			cd		
nl	chops	Osm.	Salt	Urea	Osm.	Salt	Urea	Osm.	Salt	Urea	Osm.	Salt	Urea
20	1	2.316	1.942	5.906	2.333	2.453	2.259						
10	2							2.275	1.718	7.620	2.288	2.638	2.072
30	1	2.318	2.037	5.009	2.330	2.286	2.357						
10	3							2.282	1.723	7.645	2.295	2.650	2.076
40	1	2.310	2.086	4.455	2.314	2.151	2.415						
20	2							2.319	1.944	5.914	2.336	2.457	2.261
10	4							2.285	1.724	7.656	2.297	2.653	2.078

Using various fractions for the transmural fluxes between tubes from MN2, we get the results shown in Table 7. The first line is the result in Table 6 corresponding to nl = 40 and chops = 1, and d, ah, cd, dv, 1, and 2 denote DHL, AHL, CD, DVR, AVR1, and AVR2.

In Table 8, we have shown the results from MN3 using parameters, transmural flux fractions, and boundary values from Tables 1–3. When we increased the number of loops, the number of CDs, the number of DVRs, and the number of AVRs, CD urea concentration ratios also increased. However, as we increased chops for the same number of loops, number of CDs, number of DVRs and number of AVRs, CD urea concentration ratios did not change.

Using the same constant permeabilities from top to bottom for each DHL, AHL, CD, and DVR, the CD osmolality and urea concentration ratios corresponding to different number of loops and chops from MN2, let us call as the first case, these were shown in Figure 4. Using the variations in permeabilities for every tube, (see equation (55)), and the boundary values shown in Table 3, we got the CD osmolality and urea concentration ratios shown in Figure 4. Let us call these results as the second case. Using the variations in permeabilities from top to bottom in each tube, (see equation (56)), and the boundary values shown in Table 3, we got the CD osmolality and urea concentration ratios shown in Figure 4. Let us call these results as the third case.

7. CONCLUSIONS

It is evident that the models MN1, MN2, and MN3 are physiologically more realistic. In all models, CD urea concentration ratios increased as the number of loops, the number of CDs, the number of DVRs, and the number of AVRs were increased, and CD urea concentration ratios did not change as chops were increased for the same number of loops, number of CDs, number of DVRs, and number of AVRs (see Tables 4, 6, and 8). Moreover, adding fractional transmural fluxes between DHL and DVR, and CD and DVR also led to some improvements shown in the last two rows of Tables 5 and 7.

The parameters and boundary values used for model M1 in [15] had led to, respectively, 2.199 and 1.663 as salt and urea concentration ratios for CD. The corresponding values from MN2 are 1.043 and 2.000, and for MN1 are 0.902 and 2.210. Clearly, models MN1 and MN2 lead

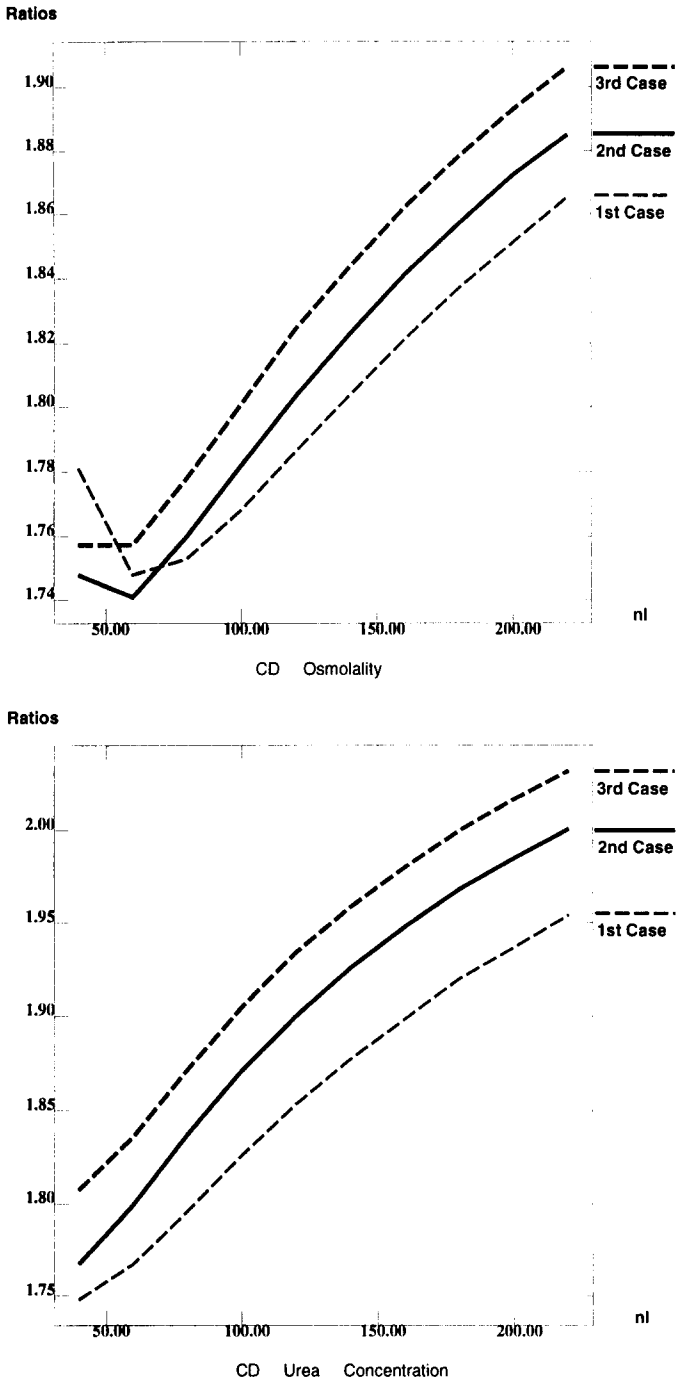

Figure 4. CD osmolality and urea concentration ratios from MN2.

to significant improvements in the concentration profiles since the CD urea concentration ratios increased and salt concentration ratios decreased, thus getting closer to experimentally observed values.

Note from Figure 4 that the CD osmolality and urea concentration ratios for the third case (second case) are higher than those for the second case (first case) for the same number of loops. These results clearly show the important role of the interstitium in the renal concentrating mechanism.

The overall computation efficiency is related directly to the size of the Jacobian, which in turn depends on the number of loops, number of CDs and number of VRs. If we assume that the

Jacobian is stored in a double precision array where each element requires eight bytes of memory, then the amount of memory needed to store the Jacobian is $8 \times [9 \times ((\mathrm{nl}-1) \times \mathrm{nl} - (\mathrm{nl} \times \mathrm{nl} - 3 \times \mathrm{nl})/2) \times \mathrm{chops}]^2$ in MN3, and $8 \times [9 \times \mathrm{nl} \times \mathrm{chops}]^2$ in MN1 and MN2. For example, in MN3, 40 nl and one or two chops need 415.5 Mb and 1662.1 Mb for the Jacobian. Thus, MN3 programs require huge memory. Therefore, we can not run the programs larger than 40 number of loops and two chops on serial computers, and need to develop *parallel programs for the multi-nephron and multi-vasa recta models* in future.

We have shown that our kidney models, based on carefully selected histotopographical and interstitial information, led to salt and urea concentrations in the final collecting duct that are very close to experimental observations.

REFERENCES

1. A. Edwards and T.L. Pallone, Facilitated transport in vasa recta: Theoretical effects on solute exchange in the medullary microcirculation, *Am. J. Physiol.* **272** (41), F505–F514, (1997).
2. E. Koushanpour and W. Kriz, *Renal Physiology,* Second Edition, Springer-Verlag, (1986).
3. I.H. Moon and R.P. Tewarson, Numerical solutions of differential equations for renal concentrating mechanism in inner medullary vasa recta models, *Computers Math. Applic.* **36** (7), 69–78, (1998).
4. J.L. Stephenson, H. Wang and R.P. Tewarson, Effect of vasa recta flow on concentrating ability of the renal inner medulla, *Amer. J. of Physiology* **268** (4), F698–F709, (1995).
5. H.E. Layton, Distribution of Henle's loops may enhance urine concentrating capability, *Biophys. J.* **49**, 1033–1040, (1986).
6. H.E. Layton, M.A. Knepper and C.L. Chou, Permeabilty criteria for effective function of passive countercurrent multiplier, *Am. J. Physiol.* **270** (39), f9–f20, (1996).
7. H.E. Layton, E.B. Pitman and M.A. Knepper, A dynamic numerical method for models of the urine concentrating mechanism, *SIAM J. Appl. Math.* **55** (5), 1390–1418, (1995).
8. K. Sun, I.H. Moon, R.P. Tewarson and J.L. Stephenson, Parallel algorithms for multi-nephron renal medullary models, *Computers Math. Applic.* **33** (6), 37–45, (1997).
9. H. Wang, J.L. Stephenson, Y. Deng and R.P. Tewarson, An efficient parallel algorithm for solving n-nephron models of the renal inner medulla, *Computers Math. Applic.* **28** (5), 1–12, (1994).
10. H. Wang, R.P. Tewarson, J.L. Stephenson and F. Jen, A comparison of multinephron and shunt models of the renal concentrating mechanism, *Appl. Math. Lett.* **6** (2), 61–65, (1993).
11. R.P. Tewarson, H.Wang, J.L. Stephenson and J.F. Jen, Efficient solution of differential equations for kidney concentrating mechanism analyses, *Appl. Math. Lett.* **4** (6), 69–72, (1991).
12. R.P. Tewarson, J.L. Stephenson and L.L. Juang, A note on solution of large sparse systems of nonlinear equations, *J. Math. Anal. and Appl.* **63**, 439–445, (1978).
13. M. Imai, J. Taniguchi and K. Yoshitomi, Transition of permeability properties along the limb of long-loop nephron, *Am. J. Physiol. (Renal Fluid Electrolyte Physiol.)* **254** (23), F323–F328, (1988).
14. M. Imai, Function of the thin ascending limb of Henle of rats and hamsters perfused in vitro, *Am. J. Physiol.* **232** (3), F201–F209, (1977).
15. J.M. Sands, H. Nonoguchi and M.A. Knepper, Vasopressin effects on urea and H_2O transport in inner medullary collecting duct subsegments, *Am. J. Physiol.* **253** (22), F823–F832, (1987).
16. J.M. Sands, H. Nonoguchi and M.A. Knepper, Hormone effects on NaCl permeability of rat inner medullary collecting duct, *Am. J. Physiol.* **255** (24), F421–F428, (1988).
17. T. Pallone, Effect of sodium cloride gradients on water flux in rat descending vasa recta, *J. Clin. Invest.* **87**, 12–19, (1991).
18. T.L. Pallone, J. Work and R.L. Jamison, Resistance of descending vasa recta to the transport of water, *Am. J. Physiol.* **259** (28), F688–F697, (1990).
19. T.L. Pallone, J. Work, R.L. Myers and R.L. Jamison, Transport of sodium and urea in outer medullary descending vasa recta, *J. Clin. Invest.* **93**, 212–222, (1994).
20. K.V. Lemley and W. Kriz, Cycles and separations: The histotopography of the urinary concentrating process, *Kidney Internat.* **31**, 538–548, (1987).
21. E. Koushappour, R.R. Tarica and W.F. Stevens, Mathematical simulation of normal nephron function in rat and man, *J. Theor. Bio.* **31**, 177–214, (1971).
22. R.P. Tewarson and I.H. Moon, Renal concentrating mechanism: Central core and vasa recta models, *Appl. Math. Lett.* **10** (2), 39–44, (1997).
23. P. Lory, Numerical solution of a kidney model by multiple shooting method, *Math. Biosci.* **50**, 117–128, (1980).
24. P. Lory, A mathematical modeling technique for renal counterflow systems, *Appl. Math. Lett.* **6** (2), 83–87, (1993).
25. R. Mejia and J.L. Stephenson, Numerical solution of multinephron kidney equations, *J. Computational Physics* **32**, 235–246, (1979).

26. R. Mejia and J.L. Stephenson, Solution of a multinephron, multisolute model of the mammalian kidney by Newton and continuation methods, *Math. Biosci.* **68**, 279–298, (1984).
27. J.L. Stephenson, Y. Zhang and R.P. Tewarson, Electrolyte, urea, and water transport in a two nephron central core model of the medulla, *Amer. J. of Physiology* **25**, F399–F413, (1989).
28. J. Strieter, A.M. Weinstein and J.L. Stephenson, A mathematical model of the rabbit thick ascending limb, Abstract, *J. Am. Soc. Nephrol.*, (1992).
29. J. Taniguchi, K. Tabei and M. Imai, Profiles of water and solute transport along long-loop descending limb: Analysis by mathematical model, *Am. J. Physiol.* **252**, F201–F209, (1987).
30. R.P. Tewarson, Basic variables in mathematical models of the kidney, *Math. Mod. and Sc. Computing* **1**, 445–449, (1995).
31. R.P. Tewarson and I.H. Moon, Efficient computational algorithms for kidney modeling, Proceedings of the *Applied Sciences, Especially Mechanics, Minisymposia,* (Edited by E. Kreuzer and O. Mahrenholtz), Special issue of *ZAAM,* **76** (Supplement 4), 51–54, (1996).